Journal of Theoretical Biology 498 (2020) 110266

Contents lists available at ScienceDirect

Journal of Theoretical Biology

journal homepage: www.elsevier.com/locate/jtb

# An approximate solution of the interferon-dependent viral kinetics model of influenza

Harald Schmid, Hana M. Dobrovolny*

*Department of Physics & Astronomy, Texas Christian University, Fort Worth, TX, USA*

ARTICLE INFO

*Article history:*
Received 23 September 2019
Revised 10 January 2020
Accepted 1 April 2020
Available online 24 April 2020

*Keywords:*
Influenza
Viral dynamics model
Magnus expansion
Approximation of nonlinear differential equations

ABSTRACT

The analysis of viral kinetics models is mostly achieved by numerical methods. We present an approach via a Magnus expansion that allows us to give an approximate solution to the interferon-dependent viral infection model of influenza which is compared with numerical results. The time of peak viral load is calculated from the approximation and stays within 10% in the studied range of interferon (IFN) efficacy $\epsilon \in [0, 1000]$. We utilize our solution to interpret the effect of varying IFN efficacy, suggesting a competition between virions and interferon that can cause an additional peak in the usually exponential increase in the viral load.



## 1. Introduction

The interplay of mathematical modeling and experiment resulted in a major change in the current understanding of the human immunodeficiency virus (HIV) as well as medical treatment after infection (Perelson and Nelson, 1999). Modeling infectious diseases has attracted much attention since then, extending the method successfully to hepatitis B and C (Nowak et al., 1996; Neumann et al., 1998), influenza (Baccam et al., 2006; Dobrovolny et al., 2013), respiratory syncytial virus (González-Parra and Dobrovolny, 2015; 2018), ebola (Nguyen et al., 2015; Madelain et al., 2018), and other viruses (González-Parra et al., 2018; Pires de Mello et al., 2018; Asquith and Bangham, 2007; Clapham et al., 2014; Gallegos et al., 2016). However, the equations used in viral kinetic models are often nonlinear and exclude closed analytic solutions for quantities comparable with experiment. Approximate solutions can be helpful to check and interpret the numerical results (Smith et al., 2010).

In mathematical models of infections one usually focuses on the macroscopic observables and describes their time evolution by rate equations. For the persistent diseases HIV and hepatitis B and C, the mentioned observables are the susceptible target cells $T$ and the infected cells $I$, which produce the virions $V$. For influenza it was shown that a separation of the infected cells in a group called the eclipse cells $I_1$ and active infected cells $I_2$ produces more accurate numerical results (Baccam et al., 2006) due to the fact that progeny virions are not detected for 6 to 8 h after infection (Sedmak and Grossberg, 1973).

Models incorporating various facets of the immune response have also been proposed (Dobrovolny et al., 2013). The adaptive immune response typically takes several days to appear and has little effect on the early viral time course (Beauchemin and Handel, 2011; Dobrovolny et al., 2013), but the innate response arises much more quickly. Although it contains many different components, the innate immune response is typically represented in mathematical models by interferon (IFN) (Dobrovolny et al., 2013; Pawelek et al., 2012). IFN has an effect on the early time course of viral load of influenza as it is actively produced 24 h after the infection (Roberts et al., 1979). IFN has a number of effects on biological processes that occur during an influenza infection such as interfering with synthesis and/or translation of viral RNA (Samuel, 2001), increasing cell apoptosis (Balachandran et al., 2000; Kuriakose et al., 2018), inducing natural killer cells (Biron et al., 1999; Kronstad et al., 2018; Jegaskanda et al., 2018), and inducing resistance to infection in cells (Guo et al., 2019; Bedford et al., 2019). Mathematical models have incorporated the effect of IFN in a variety of ways, starting with Ref. Baccam et al. (2006) where an interferon-dependent model of influenza was used to explain the occurrence of bimodal virus titer curves. More recent models have also examined the effect of IFN on the viral titer either on its own or (Pawelek et al., 2012; Handel et al., 2010; Saenz et al., 2010; Leviyang and Griva, 2018) in conjunction with other immune responses (Bocharov and Romanyukha, 1994; Hancioglu et al., 2007; Handel et al., 2018; Yan et al., 2017; 2016; Price et al., 2015). De-

* Corresponding author.
*E-mail address:* h.dobrovolny@tcu.edu (H.M. Dobrovolny).

https://doi.org/10.1016/j.jtbi.2020.110266
0022-5193/

spite the success that was achieved modeling influenza, all of the mentioned results but one for the simplest case of influenza kinetics without an immune response (Ref. Smith et al., 2010) are numerically achieved.

In this paper we derive an approximate solution to the interferon-dependent model for influenza with a method known as the Magnus expansion. In Section 2 we introduce the interferon-dependent mathematical model used for studying influenza kinetics and we present the numerical results for the viral titer and the time of peak viral load. Section 3 outlines preparing observations and steps towards the approximate solution. In Section 4 we apply a Magnus expansion to the model, obtaining an approximation formula for the viral load, which helps us to interpret the effect of interferon on the time evolution of viral load. We then use the approximation to compute the time of peak viral load. After a discussion of our results in Section 5, we give some mathematical details in Appendix A.

## 2. Mathematical model and numerical analysis

We introduce the system of ordinary differential equations, used to describe virus infection kinetics of influenza incorporating interferon response (Baccam et al., 2006),

$$\dot{T} = -\beta(F)\,TV \tag{1a}$$

$$\dot{E} = \beta(F)\,TV - kE \tag{1b}$$

$$\dot{I} = kE - \delta I \tag{1c}$$

$$\dot{V} = p(F)\,I - cV \tag{1d}$$

$$F = \frac{2}{e^{\lambda_d (t-t_p)} + e^{-\lambda_g (t-t_p)}}. \tag{1e}$$

$T$ is the amount of uninfected target cells and $V$ is the viral titer. The infected cells are split into two distinct populations: the eclipse cells $E$ which are infected but not yet producing virions, and the population $I$ which is actively producing virions. This delay in the virus productivity accounts for various intracellular processes (Pinky and Dobrovolny, 2016). The amount of interferon (Type I IFN) is denoted by $F$. Type I IFN mediates antiviral defense mechanisms through activation of cell-intrinsic mechanisms that operate in the infected cells (Gamblin and Skehel, 2010). The target cells $T$ are infected at a rate $\beta(F)TV$ whereupon they become eclipse cells $E$; the latter become active infectious cells $I$ in a characteristic transition time $1/k$. The infectious cells $I$ produce virions at a rate $p(F)I$ and are depleted after a time $1/\delta$. The virions are cleared at a rate $cV$. We choose to model the time course of interferon using a functional formulation as in (Quirouette et al., 2020). The time course of interferon $F$ typically exhibits a steep rise in the beginning due to its production by infectious cells with characteristic growth time $1/\lambda_g$ until an approximate peak time $t_p$. After the peak it is depleted by binding to cellular IFN receptors, which are internalized, or through degradation (Baccam et al., 2006) in a time $1/\lambda_d$ (Baccam et al., 2006; Dobrovolny et al., 2013; Pawelek et al., 2012; Quirouette et al., 2020).

We model the effect of interferon $F$ on the infection of target cells and the production of virus through the functions $\beta(F)$ and $p(F)$, respectively, similar to the effect of a drug as

$$\beta(F) = \frac{\tilde{\beta}}{1+\epsilon F}, \quad p(F) = \frac{\tilde{p}}{1+\eta F}, \tag{2}$$

with $\tilde{\beta}$ and $\tilde{p}$ corresponding to the case without interferon and $\epsilon$ and $\eta$ two free parameters, connected to the IFN effectiveness (Canini and Perelson, 2014). In contrast to the other parameters in Eq. (1), we vary $\epsilon$ and $\eta$ in a range of $\epsilon$, $\eta \in [0, 1000]$ (Baccam et al., 2006; Pawelek et al., 2012; Handel et al., 2010; 2018; Cao et al., 2015; Cao and McCaw, 2017), in order to obtain the time, $t_{peak}$, associated with the peak viral load $V_{peak}$, $V(t_{peak}) = V_{peak}$. This will give us a measure of accuracy of our approximate solution of the viral load.

We investigate the time course of the quantities in our model numerically (Fig. 1) in a range up to 15 days. First, we choose $p(F) = \tilde{p}$, meaning $\eta = 0$, and recover a qualitatively similar behavior for different values of $\epsilon < 100$: an exponential increase (phase 1) followed by an exponential decrease (phase 2) in agreement with Ref. Baccam et al. (2006). However, the effect of interferon causes a delay of the exponential increase in phase 1 in the very beginning, while it makes no difference in phase 2.

For $\epsilon > 100$, phase 1 is modified: The curvature of the growth phase is modified by the appearance of a saddle point (magenta curve for $\epsilon = 300$), transforming into a second local maximum before the viral peak (red curve for $\epsilon = 1.e+03$). Now looking at the effect of $p(F)$, maintaining $\beta(F) = \tilde{\beta}$ fixed ($\epsilon = 0$), we observe a qualitatively similar behavior with one exception: The viral peak shrinks with increasing $\eta$ until $\eta \approx 100$ and rises again from $\eta > 100$ on.

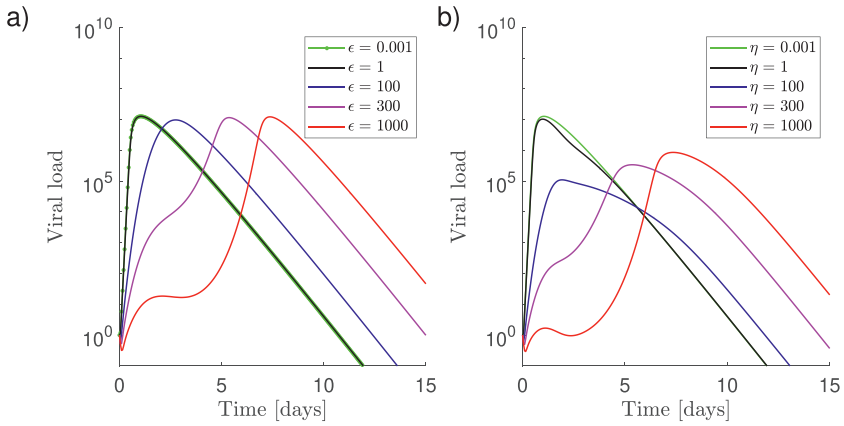


**Fig. 1.** Numerical results for the interferon-dependent model (Eq. (1)). **(a)** The time-course of the viral load is plotted for different values of $\epsilon$ and setting $\eta = 0$ ($p(F) = \tilde{p}$). All green, black and blue curves show an exponential increase (phase 1) of viral load until a maximum $V_{peak}$ is reached and then an exponential decay until the infection duration time $V(T)$ (phase 2). For $\epsilon > 100$, phase 1 is modified such that a saddle point is formed (magenta curve for $\epsilon = 300$), which transforms into a second local maximum before the viral peak (red curve for $\epsilon = 1000$). The exponential decrease of phase 2 stays the same but is delayed in time. For an explanation of the formation of the second peak, see Section 5. **(b)** Fixing $\beta(F) = \tilde{\beta}$ ($\epsilon = 0$) varying $\eta$ reveals a qualitatively similar behavior, although the value of viral peak load changes. (For interpretation of the references to color in this figure legend, the reader is referred to the web version of this article.)

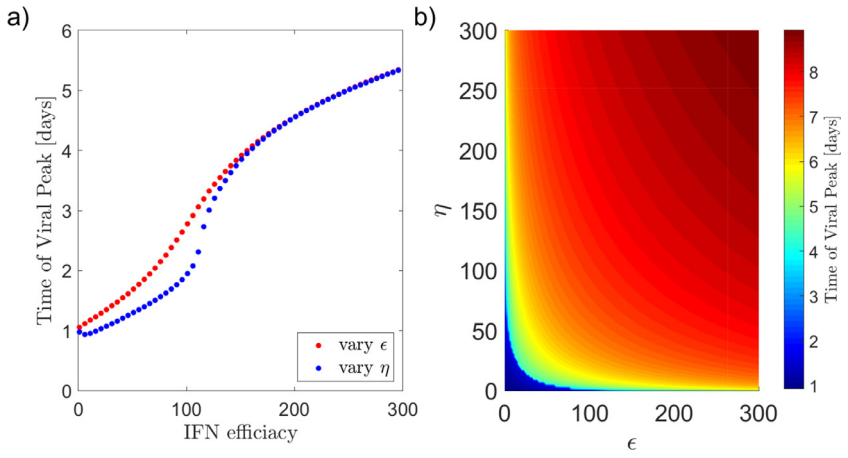


**Fig. 2.** Numerical results for the time of peak viral load. **(a)** We show the dependence of peak viral load on IFN efficiency parameters $\epsilon$ and $\eta$. The red curve was obtained by setting $\eta = 0$ and varying $\epsilon$, and the blue curve the other way around. As expected from Fig. 1, both show a similar behavior, increasing for most of chosen range of $\epsilon$ and $\eta$. Both change their curvature around $\epsilon, \eta \approx 100$, which is the region where the saddle point in Fig. 1 forms. **(b)** The contour plot shows the variation of both $\epsilon$ and $\eta$. (For interpretation of the references to color in this figure legend, the reader is referred to the web version of this article.)

Again fixing $\eta = 0$ and varying $\epsilon$ ($t_{\text{peak}}(\epsilon, \eta = 0)$), and the other way around ($t_{\text{peak}}(\eta, \epsilon = 0)$) we compute the time of peak viral load Fig. 2. For both scenarios we obtain an increasing time of viral peak with increasing IFN efficiency parameter, where the qualitative behavior is independent of which parameter is fixed and which varied. Both graphs have an inflection point around $\eta$, $\epsilon \approx 100$. For $\eta, \epsilon > 150$ the values of the time of viral peak match $t_{\text{peak}}(\epsilon, \eta = 0) \approx t_{\text{peak}}(\eta, \epsilon = 0)$. We therefore simplify our upcoming analysis by considering only $\beta(F(t))$ and $p = \tilde{p}$ fixed.

## 3. Preliminary analysis

An approximated solution for the infected cells in the interferon-independent case is derived in Ref. Smith et al. (2010). Similarly, we split the observation time $t$ in our model into a phase 1 ($T(t) \approx T_0$) and a phase 2 ($T(t) \approx 0$). Formally, we justify this by integrating Eq. (1a), thus reducing the number of equations from five to four:

$$T(t) = T_0 \exp\left(-\int_0^t \mathrm{d}t'\, \beta(F) V(t')\right). \tag{3}$$

For $t$ sufficiently small, $T \approx T_0$, and we define the time $t_{\text{split}}$ which splits phase 1 ($t < t_{\text{split}}$) and phase 2 ($t > t_{\text{split}}$) by

$$\int_0^{t_{\text{split}}} \mathrm{d}t'\, \beta(F(t')) V(t') = 1. \tag{4}$$

This definition can be mathematically motivated: From the IFN-independent solution we know that for times $t < t_{\text{split}}$ the viral load is exponentially increasing $V(t) \sim e^{\gamma t}$ for some $\gamma > 1$. We will show later that our approximated solution (Eq. (21)) is exponentially increasing. Because the integral of an exponential is an exponential, we have $T \sim \exp(\gamma_1 \exp(\gamma_2 t))$ for some $\gamma_1$ and $\gamma_2$. One definition of the Heaviside function $H(x)$ (Abramowitz et al., 1966) is

$$H(x) = \lim_{a \to 0} e^{-e^{-x/a}}, \quad H(0) = 1/e. \tag{5}$$

The Heaviside function is a good functional approximation for the target cells $T$ since we can relate the parameters $\gamma_1 \approx \sqrt[3]{b} - a \gg 1$ where $a$ and $b$ will be introduced in Eq. (17). This mathematical argument is in line with a similar definition given by Smith et al. (2010) who define the splitting time $t_{\text{split}}$ to be the time when $T$ reaches 10% of its initial value. In this work we focus on an approximated phase 1 solution, since the solution for phase 2 is the same as in the interferon-independent two-phase model in Smith et al. (2010) (we derive an explicit form of the phase 2 approximation in Section A.2). Taking a look at the parameters in Table 1, we notice the following relation concerning orders of magnitude for influenza:

$$c, k, \delta \ll \tilde{\beta} \times \tilde{p} \times T_0 \tag{6}$$

This statement seems to be generally true for a wide range of papers of modeling influenza viral kinetics (Baccam et al., 2006; Pawelek et al., 2012; Cao et al., 2015; Cao and McCaw, 2017; Pinky and Dobrovolny, 2016; Yan et al., 2016; Saenz et al., 2010). We will also need the similar statement in the following,

$$c, k, \delta \ll \beta(F(t)) \times \tilde{p} \times T_0, \tag{7}$$

which is only true for $\epsilon < 100$[1] and all considered measurement times $t$. Both conditions (6) and (7) will enter in the derivation of the approximate solution. To obtain another relation concerning the order of parameters, we rescale our model in the following manner:

$$V \mapsto V_{\text{new}} = T_0 V \quad \tilde{p} \mapsto \tilde{p}_{\text{new}} = T_0 \tilde{p}. \tag{8}$$

This leaves us with another relation concerning our new re-scaled parameters,

$$\tilde{\beta} \ll c, k, \delta \ll \tilde{p}_{\text{new}}. \tag{9}$$

**Table 1**
Parameters and starting conditions for Eq. (1). The parameters and initial values of the different quantities (where $T(0) = T_0, E(0) = E_0, \ldots$) for modeling influenza are taken mostly from the model proposed by Pawelek et al. (2012) which has no eclipse phase $E$. In agreement with models that include this additional phase (Pinky and Dobrovolny, 2016; Saenz et al., 2010; Baccam et al., 2006), the value of $k$ and $\delta$ were chosen to be same. The parameters $\lambda_g$, $\lambda_d$ were chosen according to Quirouette et al., 2020, while $t_p$ was set to 2 days based on experimental data from human and horse (Hayden et al., 1998; Saenz et al., 2010). The initial interferon load depends on the units measured and is usually normalized to 1 (Cao and McCaw, 2017; Pawelek et al., 2012). By varying the two IFN efficiency parameters $\epsilon$ and $\eta$ in a range of two orders of magnitude larger than in the Pawelek-model we compensate for the small value of $F_0$.

| $k$ [1/d] | $\delta$ [1/d] | $c$ [1/d] | $\tilde{\beta}$ [1/d] | $\tilde{p}$ [1/d] | $\lambda_d$ [1/d] | $\lambda_g$ [1/d] |
|---|---|---|---|---|---|---|
| 2 | 2 | 15 | 4.70e−05 | 5.3e−3 | 1 | 2 |
| $t_p$, [d] | $T_0$ | $E_0$ | $I_0$ | $V_0$ | $F_0$ | |
| 2 | 1.e+11 | 0 | 0 | 1 | 3.65[2] | |

[1] We define here $a \ll b$ if $a/b \leq \mathcal{O}(10^{-2})$.

Note also, that this re-scaling changes nothing about our previous relation Eq. (7). We rewrite the resulting equations for $x = (E, I, V_{\text{new}})^{\mathrm{T}}$ during phase 1 in matrix form

$$\frac{\mathrm{d}}{\mathrm{d}t}x(t) = A(t)x(t), \quad A(t) = \begin{pmatrix} -k & 0 & \beta(t) \\ k & -\delta & 0 \\ 0 & \tilde{p}_{\text{new}} & -c \end{pmatrix}, \tag{10}$$

which is the form we need for solving as a Magnus expansion.

## 4. Application of the Magnus expansion

An exact, but formal solution of Eq. (10) can be given on the one hand by a Dyson series (Dyson, 1949)

$$x(t) = \mathcal{T}\left(\exp \int_0^t \mathrm{d}t' A(t')\right), \tag{11}$$

which is often used in perturbative quantum field theory (with $\mathcal{T}$ denoting the time-ordering operator), or on the other hand by a Magnus expansion (Magnus, 1954),

$$x(t) = \exp\left(\Omega(t)\right), \quad \Omega(t) = \sum_{k=1}^{\infty} \Omega_k(t). \tag{12}$$

Practically, one truncates the Dyson series as well as the Magnus expansion after a finite number of terms. Because we already know that the numerical data initially exhibits an exponential increase preceded by a small delay in the beginning, we will use the Magnus expansion for approximating our phase 1 solution here.

Following Section A.1, the important integral that has to be done for calculating $\Omega_1$, is :

$$f(t) \equiv \int_0^t \mathrm{d}t_1 \frac{1}{1 + \epsilon F(t_1)}. \tag{13}$$

We integrate Eq. (13) numerically and state $\Omega_1$:

$$\Omega_1 = \begin{pmatrix} -kt & 0 & \tilde{\beta} f(t) \\ kt & -\delta t & 0 \\ 0 & \tilde{p}_{\text{new}} t & -ct \end{pmatrix}. \tag{14}$$

If we truncate the Magnus series at the first term, we need to diagonalize $\Omega_1$ in order to evaluate its exponential. The eigenvalues are computed by solving the secular equation:

$$0 = -\det(\Omega_1 - \lambda \mathbb{I}_{3\times 3}) \tag{15a}$$

$$= \lambda^3 + t(c + k + \delta)\,\lambda^2 + t^2(k\delta + kc + \delta c)\,\lambda + t^2 k(\delta c t - \tilde{p}_{\text{new}}\tilde{\beta} f(t)). \tag{15b}$$

This can be solved by the standard method of Cardano. Taking the orders of magnitude of our parameters (Eqs. (6)–(9)) into account, we find an approximation for our three eigenvalues $\lambda_0(t) \in \mathbb{R}$ and $\lambda_+(t), \lambda_-(t) \in \mathbb{C}$

$$\lambda_0 = \sqrt[3]{b f(t)\, t^2} - at, \; \lambda_+ = \sqrt[3]{b f(t)\, t^2}\, e^{\frac{2\pi i}{3}} - at, \; \lambda_- = \sqrt[3]{b f(t)\, t^2}\, e^{-\frac{2\pi i}{3}} - at, \tag{16}$$

with the parameters

$$a = \frac{c + k + \delta}{3}, \quad b = k\tilde{p}_{\text{new}}\tilde{\beta} = k\tilde{p}\tilde{\beta}T_0. \tag{17}$$

The components $v_j^x, v_j^y, v_j^z$ of the orthonormalized eigenvectors $v_j \in \mathbb{C}^3$, $j = \{0, +, -\}$ associated with the eigenvalues $\lambda_0, \lambda_+, \lambda_-$ are:

$$v_j^z(t) = \frac{1}{\sqrt{1 + \left(\frac{\tilde{\beta} f(t)}{\lambda_j + kt}\right)^2 + \left(\frac{ct + \lambda_j}{\tilde{p}_{\text{new}} t}\right)^2}}, \quad v_j^x(t) = \frac{\tilde{\beta} f(t)}{\lambda_j + kt} v_j^z,$$
$$v_j^y(t) = \frac{ct + \lambda_j}{\tilde{p}_{\text{new}} t} v_j^z. \tag{18}$$

Further we determine the vector $r = (r_1, r_2, r_3)^{\mathrm{T}}$ in Eq. (A.6) which corresponds to our initial conditions. At time $t = 0$, the eigenvalues vanish, $\lambda_j(0) = 0$. It also holds for the combinations $(v_j^x)^2$, $v_j^x \cdot v_j^y$, $(v_j^y)^2 \ll v_j^x \cdot v_j^z$, $v_j^y \cdot v_j^z \ll (v_j^z)^2$ and $v_j^z(0) \approx 1$. We can compute

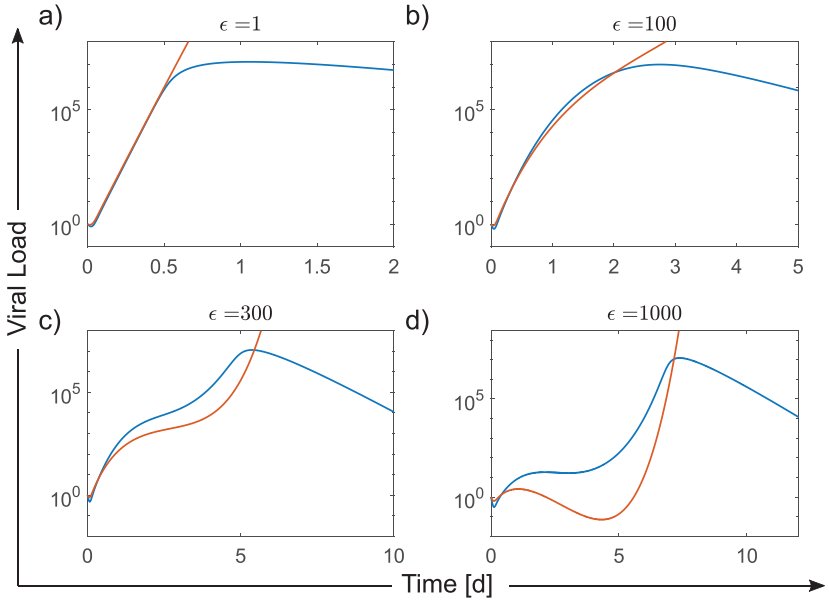


**Fig. 3.** An approximated solution of phase 1 by a Magnus expansion (red) for different values of the IFN efficiency $\epsilon$ and fixed $\eta = 0$. **(a)** The Magnus solution (red) for $\epsilon = 1$ truncated at the first term $\Omega_1$ gives a good approximation to the numerical data (blue) in phase 1 of the viral model of influenza. **(b)** For $\epsilon = 100$ the approximation is still very good. **(c)** For $\epsilon = 300$ the truncation of the Magnus expansion deviates from the numerical data, but around the time of peak the approximation intersects the numerical data. The Magnus solution also forms a saddle point like in the numerical data. **(d)** Although the Magnus solution seems to deviate strongly, the course of the approximation also exhibits a second local maximum. Again both curves intersect at the time of peak viral load. It is surprising that the Magnus solution shows the same qualitative behavior as the numerical solution because the approximation only holds for $\epsilon < 100$ (see Eq. (7)). (For interpretation of the references to color in this figure legend, the reader is referred to the web version of this article.)

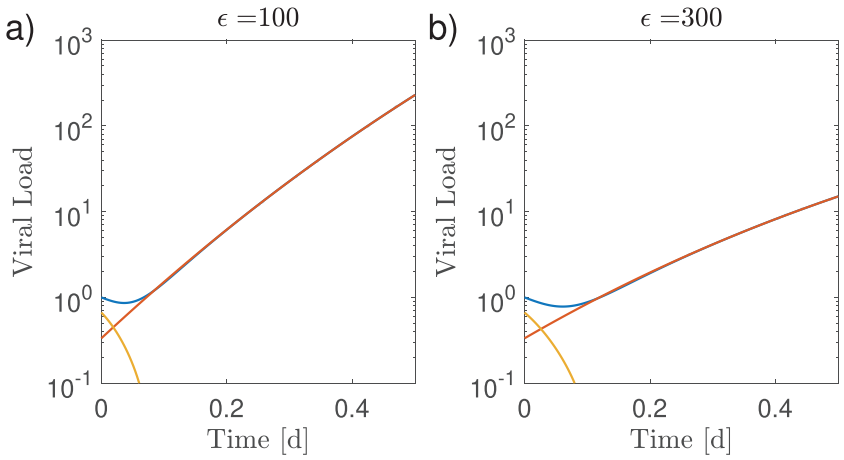


**Fig. 4.** Contribution of the first $V_{exp}$ and second summand $V_{osc}$ of the Magnus solution. The full Magnus solution (red) is composed of the exponential $V_{exp}$ (blue) and the oscillating part $V_{osc}$ (yellow). For the two different values of the Interferon efficacy their contribution is compared. Because the relation $V_{osc}/V_{exp} \leq 2e^{-3/2\sqrt[3]{bf(t)t^2}}$ holds we can ignore $V_{osc}$ without reducing the quality of the approximation for larger times. (For interpretation of the references to color in this figure legend, the reader is referred to the web version of this article.)

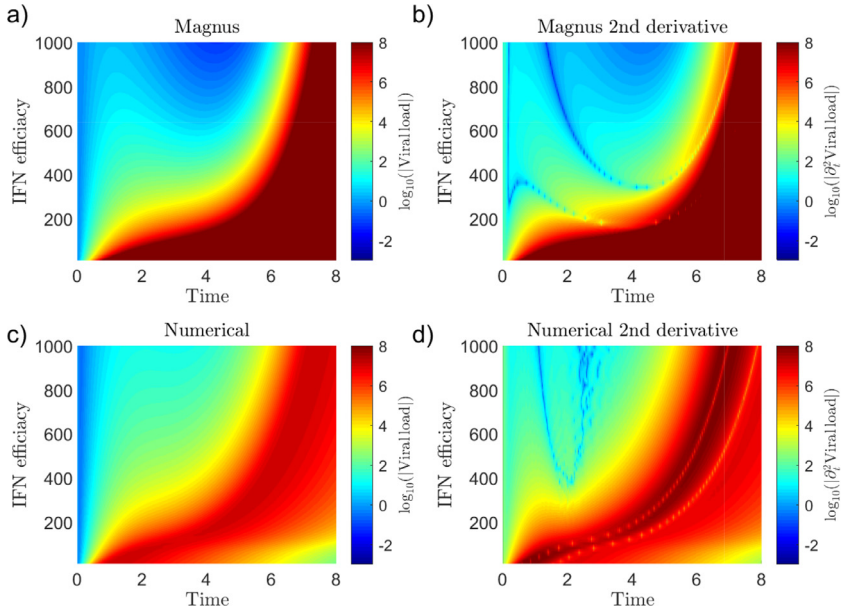


**Fig. 5.** Viral load and its second derivative in the Magnus solution and the numerical data. **(a), (c)** Although the Magnus solution is valid by definition only for $\epsilon < 100$, the graph of the numerical data in Subfig. **(a)** and the Magnus solution match for the range of $\epsilon < 500$ until the viral peak (red region in **(c)**, in agreement with the curves shown in Fig. 3. The formation of a second peak in the range of $\epsilon > 500$ is stronger in the Magnus solution compared to the numerical data (dark blue region in the north of **(a)**). **(b), (d)** The second derivative in time of the Magnus solution and the numerical data was computed numerically. The Magnus solution changes its curvature heavily before the viral peak for $\epsilon > 200$ (blue region in the north in **(b)**), which is seen as a second local maximum. However, the numerical data exhibits only a small change of curvature (light blue bow in the north in **(d)**), which is seen as inflection point in the viral load before the viral peak. (For interpretation of the references to color in this figure legend, the reader is referred to the web version of this article.)

$$(0,0,1)^{\mathrm{T}} = (v_0, v_-, v_+)(0)\,\mathrm{diag}\left(e^{\lambda_0}, e^{\lambda_-}, e^{\lambda_+}\right)(0)(v_0, v_-, v_+)^{\dagger}(0)r \tag{19}$$

$$= (v_0, v_-, v_+)(0)(v_0, v_-, v_+)^{\dagger}(0)r \approx \mathrm{diag}(0,0,3)r \tag{20}$$

where we have neglected all terms smaller than $v_j^z(0)$ in the second line. Thus we can deduce $r_3 = 1/3$ and $r_1$, $r_2$ undetermined. We set $r_1, r_2 = 0$ for simplicity. We are now ready to state a closed, approximate solution for $V(t)$ in phase 1:

$$V(t) = V_{exp}(t) + V_{osc}(t) = \frac{V_0}{3} e^{\sqrt[3]{bf(t)t^2} - at} + \frac{2V_0}{3}\cos\left(\frac{\sqrt{3}}{2}\sqrt[3]{bf(t)t^2}\right) e^{-\frac{1}{2}\sqrt[3]{bf(t)t^2} - at}, \tag{21}$$

with the parameters $a$ and $b$ given by Eq. (17).

### 4.1. Interpretation of the Magnus solution

The first summand $V_{exp}$ of the Magnus solution (Eq. (21)) is an exponentially increasing term, dominating for large enough times and causing the exponential increase. The second summand $V_{osc}$ is an exponentially decreasing oscillation term, dominating for small enough times causing a small delay in the beginning Fig. 5. For the relative contribution the relation $V_{osc}/V_{exp} \leq 2e^{-3/2\sqrt[3]{bf(t)t^2}}$ is valid, so we can safely neglect the second summand $V_{osc}$ without significantly reducing the quality of approximation when inspecting the viral peak time (Fig. 4). It is illuminating to

look at the limit

$$\lim_{\epsilon\to 0} V(t) = \frac{V_0}{3} e^{\left(\sqrt[3]{b}-a\right)t} + \frac{2V_0}{3}\cos\left(\frac{\sqrt{3}\sqrt[3]{b}}{2}t\right) e^{-\left(\sqrt[3]{b}/2+a\right)t} = V^{\text{ind}}. \tag{22}$$

This yields the interferon-independent phase 1 solution of the two-phase solution stated in Smith et al. (2010). Comparing $V^{\text{ind}}$ with $V$, interferon postpones the time at which the first term dominates (due to $\sqrt[3]{b}t \to \sqrt[3]{bf(t)\,t^2}$ and $f(t) \le t$) and slows down slightly the exponential growth, which asymptotically converges to the interferon-independent one. For $\epsilon > 100$, the second term becomes more important, revealing the formation of a second local maximum. Although the Magnus solution was derived by assuming $\epsilon < 100$ (Eq. (6)), the Magnus solution shows similar qualitative behavior as the numerical data for large $\epsilon$ and intersects the numerical data at the time of viral peak.

### 4.2. The time of peak viral load in the Magnus solution

We would like to check how accurate our obtained approximate solution is. This is achieved by calculating the time of peak viral load, testing if we recover a similar logarithmic behavior as seen in Fig. 1. In Section A.2 we derive peak viral load time $t_{\text{peak}}$ from the phase 1 solution,

$$t_{\text{peak}} = t_{\text{split}} + \Delta(\tilde{E}, \tilde{I}, \tilde{V}). \tag{23}$$

We obtain $t_{\text{split}}$ from the condition on the target cells

$$T(t_{\text{split}}) = T_0 - I(t_{\text{split}}) - E(t_{\text{split}}) = T_0/e, \tag{24}$$

which is equivalent to Eq. (4), and solve numerically. Having $t_{\text{split}}$, we can determine $\Delta$. It turns out, that $\Delta$ is approximately independent of $\epsilon$ (see Section A.2), so we can set up yet another, simpler condition for the viral load: We compute $\tilde{V}_{\text{ind}}$ for the interferon-independent viral load $V_{\text{ind}}(t)$ and demand

$$\tilde{V}_{\text{ind}} = V(t_{\text{split}}). \tag{25}$$

We can assume further that $V(t_{\text{split}}) = V_{\text{ind}}(t_{\text{split}})$, supported by the numerical data (Fig. 1). This condition for the viral load also leads us to a transcendental equation and we solve numerically. As depicted in Fig. 6, both conditions give a monotonically increasing peak time with increasing $\epsilon$. The condition on the viral load (Eq. (25)) gives a better approximation for $\epsilon < 150$, while the condition on the target cells deviates for $\epsilon < 150$ from the exact result by about a half day. Both curves exhibit the change of left to right curvature with variation of the IFN efficiacy around $\epsilon \approx 100$. The error between numerical data and Magnus approximation stays within less than 10% within a wide range of $\epsilon$.

### 4.3. Issues with higher order terms

The Magnus expansion for our approximate solution (Eq. (21)) was truncated right after the first term. We tried to calculate higher order terms $\Omega_2, \Omega_3, \ldots$ to decrease the error between the Magnus solution and the numerical data. The computation of higher order terms suggests that our ansatz (Eq. (12)) is asymptotically divergent: Taking the second order term ($\Omega_2$) into account, we obtain the same eigenvalues as in the first order (Eq. (16)). The eigenvectors change sightly, but do not affect our solution. The third order (including $\Omega_3$) gives eigenvalues that show a deviation of several orders of magnitude from the ones we have in the first order. This is of course not a formal proof of divergence, but it gives a hint that we probably work with a divergent ansatz with the Magnus expansion. The behavior of a series which gives a good approximation in some finite order, but is divergent as a whole, is known as asymptotically divergent (Boyd, 1999).

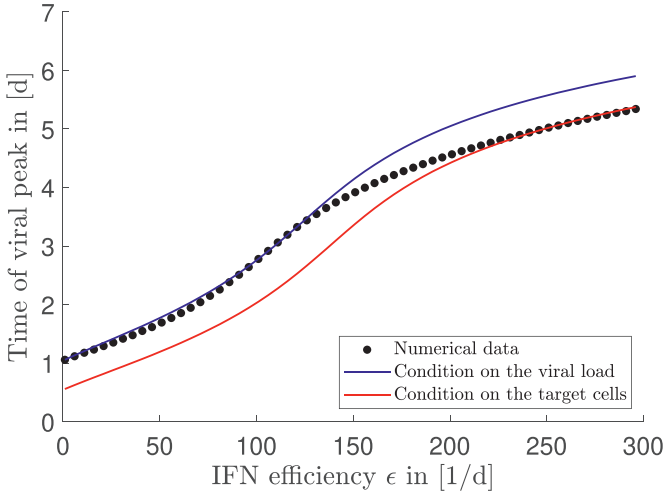


**Fig. 6.** Time of peak viral load in the Magnus solution. The conditions in Eq. (24) (red) and Eq. (25) (blue) were used to determine the peak viral load of the Magnus solution. Both conditions show the monotonically increasing behavior as recovered in the numerical data. The condition on the target cells is half a day off for $\epsilon < 200$ and approaches the numerical data. The condition on the viral load is within an error of 10% for the whole investigated range of IFN efficacy. (For interpretation of the references to color in this figure legend, the reader is referred to the web version of this article.)

## 5. Discussion and conclusion

We found an approximate solution for an interferon-dependent model for influenza with perturbation methods. We first studied the dynamics of the viral load numerically by taking experimentally measured parameters into account. We varied the IFN efficacy parameters $\epsilon$ and $\eta$ connected to parameters of the viral production rate $p$ and target cell depletion rate $\beta$ separately (Fig. 1) and simultaneously (Fig. 2). Both revealed an increasing time of peak viral load with increasing IFN efficacy and also a qualitatively similar behavior. While the peak viral load stayed nearly the same with variation of $\epsilon$ it varied with $\eta$. The exponential increase after infection was recovered only for small $\epsilon$ and $\eta$. For larger IFN efficacy the phase I curvature changed a lot and a second peak was formed. The decreasing viral load after infection was not altered by interferon.

We explain the formation of the second peak caused by large IFN efficacy in the following. The interferon load was modeled by a fast increasing and then decreasing function (Eq. (1e)) with a peak interferon load around the second day after infection. This is consistent with experimental measurements of the IFN response during influenza infection (Dobrovolny et al., 2013; Quirouette et al., 2020). Looking at the viral load during its time evolution for high IFN efficacy ($\epsilon > 500$), as the viral load increases the amount of interferon also increases. A high efficacy reduces the production rate $p$. This leads to a reduction in viral load, only if the efficacy is large enough. As time passes, virions deplete the interferon again in a characteristic time $1/\lambda_d$. A local minimum of the viral load is reached around the IFN peak time. After the IFN peak time the amount of IFN shrinks again. Finally, the virions succeed and rise exponentially until their time of peak. This competition between virions and interferon results in an increase of the time of viral peak and quantities connected to the time of viral peak like the infection duration.

We further proceeded with a derivation of an approximate solution of the proposed interferon-dependent model. Building on the two phase approximation, we could provide an approximate solution in terms of the Magnus expansion in first order that comes close to our numerical data of the model. With the help of the

retrieved solution we were able to give an interpretation of the effect of IFN. The approximate solution interpreted and revealed the change in curvature due to the early competition of IFN and virions. The error for our solution in the stated range of the IFN effectiveness was smaller than 10%. Thus, the Magnus method provides a very good approximation to the IFN-dependent model.

Additionally, this approximation shows that the innate immune response of interferon can be seen as a small perturbation to a system without immune response. The given approximated solution states in a mathematical way the manner in which interferon adds to the system without interferon: The constant exponential increase of the interferon-independent model is manifested in a linear increasing exponent with time. In the interferon-dependent model this linear exponent is changed to a time-dependent function, the integral of our interferon function. The interferon-independent system is recovered as a special case of zero IFN-efficacy, simplifying to the phase-1 solution of Smith et al. (2010) to a simple formula (Eq. (22)).

The general method of the Magnus expansion might be furthermore applicable for modeling an immune response in terms of antibodies. Similarly to the approach adopted in Bocharov and Romanyukha (1994); Handel et al. (2010); Hancioglu et al. (2007); Lee et al. (2009), the virus clearance rate $c$ can be adjusted according to

$$c \mapsto c + k_v \frac{A(t)}{A_m}, \quad A(t) = \frac{A_m}{1 + (\frac{A_m}{A_0} - 1)e^{-\alpha t}}, \tag{26}$$

with $A_0$ and $A_m$ initial and final saturation of antibodies, $\alpha$ growth rate, $k_v$ binding capacity. Following the path taken in this work, one can make an educated guess for the target cells $T$ to get rid of the nonlinear term $TV$ and solve using the Magnus approximation. Modeling drug resistance is likewise a candidate for a possible Magnus approximation where viral models for Hepatitis C have been proposed (Conway and Perelson, 2014; Shudo et al., 2009) which use a time dependent function replacing a parameter. Generally, if a model in the ODE-governed field of viral kinetics can be proposed with a time-dependent function replacing a parameter, a Magnus expansion can be sought. The formerly stated approximate solution might be useful in more difficult problems including an approximate solution to the recently proposed PDE-model describing the localization and spread of influenza infection within the human respiratory tract (Quirouette et al., 2020).

## CRediT authorship contribution statement

**Harald Schmid:** Conceptualization, Formal analysis, Writing - original draft. **Hana M. Dobrovolny:** Project administration, Supervision, Validation, Writing - review & editing.

## Acknowledgments

HS was supported by the DAAD RISE program and the Physics with integrated Doctorate Program of the Elite Network of Bavaria (University of Regensburg).

## Appendix A. Magnus expansion and the phase 2 solution

### A1. Magnus expansion

We give a quick introduction into the method of the Magnus expansion introduced by Magnus (1954) which is - in the case of its convergence - the exact solution to a time-dependent ODE of the form (Blanes et al., 2009)

$$\frac{\mathrm{d}}{\mathrm{d}t}x(t) = A(t)x(t) \tag{A.1}$$

$$x(t) \in [0, \infty) \times \mathbb{R}^n,\ A(t) \in [0, \infty) \times \mathbb{R}^{n\times n},\ x(0) = r \in \mathbb{R}^n. \tag{A.2}$$

In viral kinetics models one is only interested in positive times $t$, equations for real, measurable quantities (e.g. viral load) which are collected in a vector $x$, and real rates stored in $A$. We start with the observation that for the scalar case, $n = 1$, Eq. (A.1) can be readily integrated:

$$x(t) = \exp\left(\int_0^t \mathrm{d}t_1 A(t_1)\right) r. \tag{A.3}$$

Magnus expressed the general solution of Eq. (A.1) in terms of the exponential of an analytic function $\Omega(t) = \sum_{k=1}^{\infty} \Omega_k(t)$,

$$x(t) = \exp\big(\Omega(t)\big)\, r. \tag{A.4}$$

The first three terms of the power series are given by

$$\Omega_1 = \int_0^t \mathrm{d}t_1 A(t_1), \tag{A.5a}$$

$$\Omega_2 = \frac{1}{2}\int_0^t \mathrm{d}t_1 \int_0^{t_1} \mathrm{d}t_2 \big[A(t_1), A(t_2)\big], \tag{A.5b}$$

$$\Omega_3 = \frac{1}{6}\int_0^t \mathrm{d}t_1 \int_0^{t_1} \mathrm{d}t_2 \int_0^{t_2} \mathrm{d}t_3 \Big(\big[A(t_1), \big[A(t_2), A(t_3)\big]\big] + \big[A(t_3), \big[A(t_2), A(t_1)\big]\big]\Big), \tag{A.5c}$$

where $[A, B] = AB - BA$ denotes the commutator. The series is interpreted as follows: $\Omega_1$ is the same contribution as in the scalar case and the only one if $[A(t_1), A(t_2)] = 0$, so the matrices commute for all times $t_1$, $t_2$. If they do not commute one has to consider nested commutators. Practically, one can truncate the power series, which gives an approximate solution if the series converges. The matrix exponential $\exp(\Omega(t))$ can be calculated decomposing $\Omega$ into its Jordan form $J$. With the matrix $P$, composed of the generalized, orthonormal eigenvectors $v_j$ of $\Omega$, and the $n$-Jordan blocks $J_m$, $m \in \{1, .., n\}$, of $J$, the Magnus solution is given by

$$x(t) = P\,\mathrm{diag}\big(e^{J_1}, \ldots, e^{J_n}\big)P^{\mathrm{T}} r. \tag{A.6}$$

### A2. Phase 2 solution and time of peak viral load

We solve Eq. (1) in the phase 2 approximation (target cells $T = 0$), defined for times $t > t_{\mathrm{split}}$ (see Eq. (4)). We impose a matching condition for phase 1 and 2 solution

$$x^{\text{phase 1}}\Big|_{t=t_{\mathrm{split}}} = x^{\text{phase 2}}\Big|_{t=t_{\mathrm{split}}} \tag{A.7}$$

and now look at the case $\delta = k$, $\delta \neq c$ (Tab. 1). By successive integration of Eq. (1b), then (1c) and (1d) we get the phase 2 solution,

$$E(t) = \tilde{E}\exp(-k(t - t_{\mathrm{split}})) \tag{A.8a}$$

$$I(t) = k\tilde{E}(t - t_{\mathrm{split}})e^{-k(t-t_{\mathrm{split}})} + \tilde{I}e^{-k(t-t_{\mathrm{split}})} \tag{A.8b}$$

$$V(t) = \frac{\tilde{p}}{c-k}\left[\tilde{I} + k\tilde{E}\left(\frac{1}{k-c} + (t - t_{\mathrm{split}})\right)\right]e^{-k(t-t_{\mathrm{split}})} + \tilde{V}e^{-c(t-t_{\mathrm{split}})}, \tag{A.8c}$$

with integration constants $\tilde{E}$, $\tilde{I}$ and $\tilde{V}$ to be determined by Eq. (A.7). The maximum viral load can be obtained by the phase 2 solution,

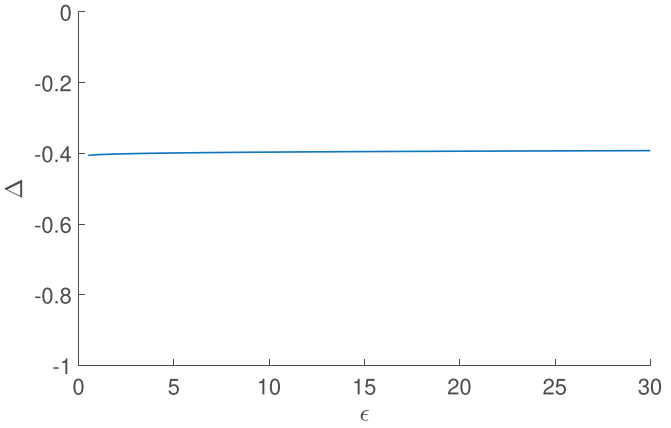


**Fig. A.7.** Dependence of $\Delta$ on the IFN efficacy $\epsilon$. $\Delta$ is nearly independent of $\epsilon$.

$$0 = \frac{\mathrm{d}}{\mathrm{d}t}V = \frac{\tilde{p}}{c-k}e^{-k(t-t_{\text{split}})}\left[-k\left(\tilde{I}+k\tilde{E}\left(\frac{1}{k-c}+(t-t_{\text{split}})\right)\right)+k\tilde{E}\right] - c\tilde{V}e^{-c(t-t_{\text{split}})} \tag{A.9a}$$

$$\Leftrightarrow e^{(k-c)(t-t_{\text{split}})} = \frac{\tilde{p}k}{c\tilde{V}(c-k)}\left[-\left(\tilde{I}+k\tilde{E}\left(\frac{1}{k-c}+(t-t_{\text{split}})\right)\right)+\tilde{E}\right] \tag{A.9b}$$

$$= \frac{\tilde{p}k}{c\tilde{V}(c-k)}\left[-\left(\tilde{I}+\frac{k\tilde{E}}{k-c}\right)+\tilde{E}\right] - \frac{k^2\tilde{E}p}{c\tilde{V}(c-k)}(t-t_{\text{split}}) \tag{A.9c}$$

Defining

$$x \equiv t - t_{\text{split}},\ g_1 = k-c,\ g_2 \equiv \frac{-k^2\tilde{E}\tilde{p}}{c\tilde{V}(c-k)},$$
$$g_3 \equiv \frac{\tilde{p}k}{c\tilde{V}(c-k)}\left[-\left(\tilde{I}+\frac{k\tilde{E}}{k-c}\right)+\tilde{E}\right] \tag{A.10}$$

leads to

$$e^{g_1 x} = g_2 + g_3 x. \tag{A.11}$$

This can be solved by defining further

$$y \equiv g_1 x, g_4 \equiv \frac{g_3}{g_1}, z \equiv -y - \frac{g_2}{g_4} \tag{A.12}$$

leading to

$$ze^{z} = -\frac{1}{g}e^{-g_2/g_4}. \tag{A.13}$$

The solution of the equation $Ye^{Y} = X$ is the Lambert-W function $Y = \mathcal{W}(X)$. When $1/e < X \leq 0$ the Lambert-W function splits into two branches $\mathcal{W}_0(X)$ and $\mathcal{W}_{-1}(X)$. For the maximum, we need $\mathcal{W}_{-1}(X)$. Substituting back, yields

$$t_{\text{peak}} = t_{\text{split}} - \frac{1}{g_1}\left\{\frac{g_2}{g_4} + \mathcal{W}\left(\frac{-e^{-g_2/g_4}}{g_4}\right)\right\} \equiv t_{\text{split}} + \Delta(\tilde{E},\tilde{I},\tilde{V}) \tag{A.14}$$

with the quantity $\Delta(\tilde{E},\tilde{I},\tilde{V})$ depending on the matching values given by Eq. (A.7). However it can be shown that $\Delta$ is approximately independent of $\epsilon$ (Fig. A.7). This is needed in the derivation of the condition for the viral peak time.

### *A3. Derivation of the approximate eigenvalues Eq. (16)*

We start with a revision of the method of Cardano. A cubic equation

$$\lambda^3 + A\lambda^2 + B\lambda + C = 0 \tag{A.15}$$

can be solved by defining

$$P = B - \frac{A^2}{3},\quad Q = \frac{2A^3}{27} - \frac{AB}{3} + C,\quad D = \left(\frac{Q}{2}\right)^2 + \left(\frac{P}{3}\right)^3 \tag{A.16}$$

and

$$u = \sqrt[3]{-\frac{Q}{2}+\sqrt{D}},\quad v = \sqrt[3]{-\frac{Q}{2}-\sqrt{D}}. \tag{A.17}$$

The three solutions are

$$z_1 = u + v - \frac{A}{3},\quad z_2 = ue^{\frac{2\pi i}{3}} + ve^{-\frac{2\pi i}{3}} - \frac{A}{3},$$
$$z_3 = ue^{-\frac{2\pi i}{3}} + ve^{\frac{2\pi i}{3}} - \frac{A}{3}. \tag{A.18}$$

We have in our case (Eq. (15))

$$A = t(c+k+\delta),\quad B = t^2(k\delta + kc + \delta c),$$
$$C = t^2k(\delta ct - \tilde{p}_{\text{new}}\tilde{\beta}f(t)). \tag{A.19}$$

By considering Eqs. (6)–(9) we can approximate

$$Q = \underbrace{2A^3/27}_{\mathcal{O}(c^3)} + \underbrace{AB/3}_{\mathcal{O}(c^3)} + \underbrace{t^3k\delta c}_{\mathcal{O}(c^3)} - \underbrace{t^2k\tilde{p}_{\text{new}}\tilde{\beta}f(t)}_{\mathcal{O}(c\tilde{p}_{\text{new}}\tilde{\beta})} \approx -t^2k\tilde{p}_{\text{new}}\tilde{\beta}f(t) \tag{A.20}$$

$$D = \underbrace{(Q/2)^2}_{\mathcal{O}((c\tilde{p}_{\text{new}}\tilde{\beta})^2)} + \underbrace{(P/3)^3}_{\mathcal{O}(c^6)} \approx (Q/2)^2 \tag{A.21}$$

and

$$u \approx 0,\quad v \approx \sqrt[3]{t^2k\tilde{p}_{\text{new}}\tilde{\beta}f(t)}. \tag{A.22}$$

Inserting this into Eq. (A.18) gives the parameters in Eq. (16).

## References


Abramowitz, M., Stegun, I., McQuarrie, D.A., 1966. Handbook of mathematical functions. Am. J. Phys. 34 (2), 177. doi:10.1119/1.1972842.

Asquith, B., Bangham, C.R.M., 2007. Quantifying HTLV-I dynamics. Immunol. Cell Biol. 85 (4), 280–286. doi:10.1038/sj.icb.7100050.

Baccam, P., Beauchemin, C., Macken, C.A., Hayden, F.G., Perelson, A.S., 2006. Kinetics of influenza a virus infection in humans. J. Virol. 80 (15), 7590–7599. doi:10.1128/JVI.01623-05.

Balachandran, S., Roberts, P.C., Kipperman, T., Bhalla, K.N., Compans, R.W., Archer, D.R., Barber, G.N., 2000. Alpha/beta interferons potentiate virus-induced apoptosis through activation of the FADD/Caspase-8 death signaling pathway. J. Virol. 74 (3), 1513–1523. doi:10.1128/JVI.74.3.1513-1523.2000.

Beauchemin, C.A., Handel, A., 2011. A review of mathematical models of influenza a infections within a host or cell culture: lessons learned and challenges ahead. BMC Public Health 11 (Suppl 1), S7. doi:10.1186/1471-2458-11-S1-S7.

Bedford, J.G., O'Keeffe, M., Reading, P.C., Wakim, L.M., 2019. Rapid interferon independent expression of IFITM3 following T cell activation protects cells from influenza virus infection. PLoS One 14 (1), e0210132. doi:10.1371/journal.pone.0210132.

Biron, C.A., Nguyen, K.B., Pien, G.C., Cousens, L.P., Salazar-Mather, T.P., 1999. Natural killer cells in antiviral defense: function and regulation by innate cytokines. Annu. Rev. Immunol. 17 (1), 189–220. doi:10.1146/annurev.immunol.17.1.189.

Blanes, S., Casas, F., Oteo, J., Ros, J., 2009. The Magnus expansion and some of its applications. Phys. Rep. 470 (5–6), 151–238. doi:10.1016/j.physrep.2008.11.001.

Bocharov, G., Romanyukha, A., 1994. Mathematical model of antiviral immune response III. Influenza a virus infection. J. Theor. Biol. 167 (4), 323–360. doi:10.1006/jtbi.1994.1074.

Boyd, J.P., 1999. The Devil's invention: asymptotic, superasymptotic and hyperasymptotic series. Acta Appl. Math. 56 (1), 1–98. doi:10.1023/A:1006145903624.

Canini, L., Perelson, A.S., 2014. Viral kinetic modeling: state of the art. J. Pharmacokinet. Pharmacodyn. 41 (5), 431–443. doi:10.1007/s10928-014-9363-3.

Cao, P., McCaw, J., 2017. The mechanisms for within-host influenza virus control affect model-based assessment and prediction of antiviral treatment. Viruses 9 (8), 197. doi:10.3390/v9080197.

Cao, P., Yan, A.W.C., Heffernan, J.M., Petrie, S., Moss, R.G., Carolan, L.A., Guarnaccia, T.A., Kelso, A., Barr, I.G., McVernon, J., Laurie, K.L., McCaw, J.M., 2015. Innate immunity and the inter-exposure interval determine the dynamics of secondary influenza virus infection and explain observed viral hierarchies. PLoS Comput. Biol. 11 (8), e1004334. doi:10.1371/journal.pcbi.1004334.

Clapham, H.E., Tricou, V., Van Vinh Chau, N., Simmons, C.P., Ferguson, N.M., 2014. Within-host viral dynamics of dengue serotype 1 infection. J. R. Soc. Interface 11 (96), 20140094. doi:10.1098/rsif.2014.0094.

Conway, J.M., Perelson, A.S., 2014. A hepatitis c virus infection model with time-varying drug effectiveness: solution and analysis. PLoS Comput. Biol. 10 (8), e1003769. doi:10.1371/journal.pcbi.1003769.

Dobrovolny, H.M., Reddy, M.B., Kamal, M.A., Rayner, C.R., Beauchemin, C.A.A., 2013. Assessing mathematical models of influenza infections using features of the immune response. PLoS One 8 (2), e57088. doi:10.1371/journal.pone.0057088.

Dyson, F.J., 1949. The radiation theories of Tomonaga, Schwinger, and Feynman. Phys. Rev. 75 (3), 486–502. doi:10.1103/PhysRev.75.486.

Gallegos, K.M., Drusano, G.L., DArgenio, D.Z., Brown, A.N., 2016. Chikungunya virus: in vitro response to combination therapy with Ribavirin and interferon Alfa 2a. J. Infect. Dis. 214 (8), 1192–1197. doi:10.1093/infdis/jiw358.

Gamblin, S.J., Skehel, J.J., 2010. Influenza hemagglutinin and neuraminidase membrane glycoproteins. J. Biol. Chem. 285 (37), 28403–28409. doi:10.1074/jbc.R110.129809.

González-Parra, G., Dobrovolny, H.M., 2015. Assessing uncertainty in A2 respiratory syncytial virus viral dynamics. Comput. Math. Methods Med. 2015, 1–9. doi:10.1155/2015/567589.

González-Parra, G., Dobrovolny, H.M., 2018. A quantitative assessment of dynamical differences of RSV infections in vitro and in vivo. Virology 523, 129–139. doi:10.1016/j.virol.2018.07.027.

González-Parra, G., Dobrovolny, H.M., Aranda, D.F., Chen-Charpentier, B., Guerrero Rojas, R.A., 2018. Quantifying rotavirus kinetics in the REH tumor cell line using in vitro data. Virus Res. 244, 53–63. doi:10.1016/j.virusres.2017.09.023.

Guo, T., Zuo, Y., Qian, L., Liu, J., Yuan, Y., Xu, K., Miao, Y., Feng, Q., Chen, X., Jin, L., Zhang, L., Dong, C., Xiong, S., Zheng, H., 2019. ADP-ribosyltransferase PARP11 modulates the interferon antiviral response by mono-ADP-ribosylating the ubiquitin E3 ligase $\beta$-TrCP. Nat. Microbiol. doi:10.1038/s41564-019-0428-3.

Hancioglu, B., Swigon, D., Clermont, G., 2007. A dynamical model of human immune response to influenza a virus infection. J. Theor. Biol. 246 (1), 70–86. doi:10.1016/j.jtbi.2006.12.015.

Handel, A., Li, Y., McKay, B., Pawelek, K.A., Zarnitsyna, V., Antia, R., 2018. Exploring the impact of inoculum dose on host immunity and morbidity to inform model-based vaccine design. PLoS Comput. Biol. 14 (10), e1006505. doi:10.1371/journal.pcbi.1006505.

Handel, A., Longini, I.M., Antia, R., 2010. Towards a quantitative understanding of the within-host dynamics of influenza a infections. J. R. Soc. Interface 7 (42), 35–47. doi:10.1098/rsif.2009.0067.

Hayden, F.G., Fritz, R., Lobo, M.C., Alvord, W., Strober, W., Straus, S.E., 1998. Local and systemic cytokine responses during experimental human influenza a virus infection. Relation to symptom formation and host defense.. J. Clin. Investig. 101 (3), 643–649. doi:10.1172/JCI1355.

Jegaskanda, S., Vanderven, H.A., Tan, H.-X., Alcantara, S., Wragg, K.M., Parsons, M.S., Chung, A.W., Juno, J.A., Kent, S.J., 2018. Influenza virus infection enhances antibody-mediated NK cell functions via Type I interferon-dependent pathways. J. Virol. 93 (5), e02090—-18. doi:10.1128/JVI.02090-18.

Kronstad, L.M., Seiler, C., Vergara, R., Holmes, S.P., Blish, C.A., 2018. Differential induction of IFN-$\alpha$ and modulation of CD112 and CD54 expression govern the magnitude of NK cell IFN-$\gamma$ response to influenza a viruses. J. Immunol. 201 (7), 2117–2131. doi:10.4049/jimmunol.1800161.

Kuriakose, T., Zheng, M., Neale, G., Kanneganti, T.-D., 2018. IRF1 is a transcriptional regulator of ZBP1 promoting NLRP3 inflammasome activation and cell death during influenza virus infection. J. Immunol. 200 (4), 1489–1495. doi:10.4049/jimmunol.1701538.

Lee, H.Y., Topham, D.J., Park, S.Y., Hollenbaugh, J., Treanor, J., Mosmann, T.R., Jin, X., Ward, B.M., Miao, H., Holden-Wiltse, J., Perelson, A.S., Zand, M., Wu, H., 2009. Simulation and prediction of the adaptive immune response to influenza a virus infection. J. Virol. 83 (14), 7151–7165. doi:10.1128/JVI.00098-09.

Leviyang, S., Griva, I., 2018. Investigating functional roles for positive feedback and cellular heterogeneity in the Type I interferon response to viral infection. Viruses 10 (10), 517. doi:10.3390/v10100517.

Madelain, V., Baize, S., Jacquot, F., Reynard, S., Fizet, A., Barron, S., Solas, C., Lacarelle, B., Carbonnelle, C., Mentré, F., Raoul, H., de Lamballerie, X., Guedj, J., 2018. Ebola viral dynamics in nonhuman primates provides insights into virus immuno-pathogenesis and antiviral strategies. Nat. Commun. 9 (1), 4013. doi:10.1038/s41467-018-06215-z.

Magnus, W., 1954. On the exponential solution of differential equations for a linear operator. Commun. Pure Appl. Math. 7 (4), 649–673. doi:10.1002/cpa.3160070404.

Neumann, A.U., Lam, N.P., Dahari, H., Gretch, D.R., Wiley, T.E., Layden, T.J., Perelson, A.S., 1998. Hepatitis C viral dynamics in vivo and the antiviral efficacy of interferon-$\alpha$ therapy. Science 282 (5386), 103–107. doi:10.1126/science.282.5386.103.

Nguyen, V.K., Binder, S.C., Boianelli, A., Meyer-Hermann, M., Hernandez-Vargas, E.A., 2015. Ebola virus infection modeling and identifiability problems. Front. Microbiol. 6. doi:10.3389/fmicb.2015.00257.

Nowak, M.A., Bonhoeffer, S., Hill, A.M., Boehme, R., Thomas, H.C., McDade, H., 1996. Viral dynamics in hepatitis B virus infection. Proc. Natl. Acad. Sci. 93 (9), 4398–4402. doi:10.1073/pnas.93.9.4398.

Pawelek, K.A., Huynh, G.T., Quinlivan, M., Cullinane, A., Rong, L., Perelson, A.S., 2012. Modeling within-host dynamics of influenza virus infection including immune responses. PLoS Comput. Biol. 8 (6), e1002588. doi:10.1371/journal.pcbi.1002588.

Perelson, A.S., Nelson, P.W., 1999. Mathematical analysis of HIV-1 dynamics in vivo. SIAM Rev. 41 (1), 3–44. doi:10.1137/S0036144598335107.

Pinky, L., Dobrovolny, H.M., 2016. Coinfections of the respiratory tract: viral competition for resources. PLoS One 11 (5), e0155589. doi:10.1371/journal.pone.0155589.

Pires de Mello, C.P., Tao, X., Kim, T.H., Vicchiarelli, M., Bulitta, J.B., Kaushik, A., Brown, A.N., 2018. Clinical regimens of favipiravir inhibit Zika virus replication in the Hollow-Fiber infection model. Antimicrob. Agents Chemother. 62 (9), AAC.00967–18. doi:10.1128/AAC.00967-18.

Price, I., Mochan-Keef, E.D., Swigon, D., Ermentrout, G.B., Lukens, S., Toapanta, F.R., Ross, T.M., Clermont, G., 2015. The inflammatory response to influenza a virus (H1N1): an experimental and mathematical study. J. Theor. Biol. 374 (374), 83–93. doi:10.1016/j.jtbi.2015.03.017.

Quirouette, C., Younis, N. P., Reddy, M. B., Beauchemin, C. A. A., 2020. A mathematical model describing the localization and spread of influenza a virus infection within the human respiratory tract. PLoS Comput. Biol. 16 (4), e1007705. doi:10.1371/journal.pcbi.1007705.

Roberts, N.J., Douglas, R.G., Simons, R.M., Diamond, M.E., 1979. Virus-induced interferon production by human macrophages. J. Immunol. 123 (1), 365–369. https://www.jimmunol.org/content/123/1/365

Saenz, R.A., Quinlivan, M., Elton, D., MacRae, S., Blunden, A.S., Mumford, J.A., Daly, J.M., Digard, P., Cullinane, A., Grenfell, B.T., McCauley, J.W., Wood, J.L.N., Gog, J.R., 2010. Dynamics of influenza virus infection and pathology. J. Virol. 84 (8), 3974–3983. doi:10.1128/JVI.02078-09.

Samuel, C.E., 2001. Antiviral actions of interferons. Clin. Microbiol. Rev. 14 (4), 778–809. doi:10.1128/CMR.14.4.778-809.2001.

Sedmak, J.J., Grossberg, S.E., 1973. Interferon bioassay: reduction in yield of myxovirus neuraminidases. J. Gen. Virol. 21 (1), 1–7. doi:10.1099/0022-1317-21-1-1.

Shudo, E., Ribeiro, R.M., Perelson, A.S., 2009. Modeling HCV kinetics under therapy using PK and PD information. Expert Opin. Drug Metab. Toxicol. 5 (3), 321–332. doi:10.1517/17425250902787616.

Smith, A.M., Adler, F.R., Perelson, A.S., 2010. An accurate two-phase approximate solution to an acute viral infection model. J. Math. Biol. 60 (5), 711–726. doi:10.1007/s00285-009-0281-8.

Yan, A.W., Cao, P., Heffernan, J.M., McVernon, J., Quinn, K.M., La Gruta, N.L., Laurie, K.L., McCaw, J.M., 2017. Modelling cross-reactivity and memory in the cellular adaptive immune response to influenza infection in the host. J. Theor. Biol. 413, 34–49. doi:10.1016/j.jtbi.2016.11.008.

Yan, A.W.C., Cao, P., McCaw, J.M., 2016. On the extinction probability in models of within-host infection: the role of latency and immunity. J. Math. Biol. 73 (4), 787–813. doi:10.1007/s00285-015-0961-5.